$H + D_2$ reaction dynamics. Determination of the product state distributions at a collision energy of 1.3 eV

Ernesto E. Marinero,[a] Charles T. Rettner,[a] and Richard N. Zare
Department of Chemistry, Stanford University, Stanford, California 94305

(Received 28 November 1983; accepted 18 January 1984)

Two-photon resonance, three-photon ionization has been used to determine the HD product internal state distribution formed by the reaction of fast H atoms with thermal D_2 molecules. A mixture of HI and D_2 is irradiated by a 266 nm laser pulse to dissociate the former, giving a center-of-mass collision energy of about 1.30 ± 0.04 eV for $H + D_2$. After a sufficiently short delay to ensure essentially collision-free conditions, a second laser is fired which causes multiphoton ionization of individual HD quantum states as well as D atoms, depending upon the choice of wavelength. Reaction occurs in a well-defined effusive flow which emerges from a glass orifice placed between the acceleration plates of a differentially pumped time-of-flight mass spectrometer. Ion signals are referenced to those obtained from HD or D produced in an auxiliary microwave discharge. Relative formation rates are reported for HD($v = 1, J = 0$–6) and HD($v = 2, J = 0$–6). Nascent D atoms are also observed and an upper limit is placed on the production of HD($v = 3$). Rotational surprisal plots are found to be linear for the HD product state distribution yielding a slope of $\theta_R = 5.1$ for HD($v = 1$) and $\theta_R = 4.7$ for HD($v = 2$). These are extrapolated to provide full distributions for HD($v = 0$–$2, J = 0$–6). The present product state distributions are compared with the recent experimental data of Gerrity and Valentini as well as with the quasiclassical trajectory calculations of Blais and Truhlar.

I. INTRODUCTION

The simplest bimolecular reaction involving neutral reagents is the hydrogen atom exchange reaction

$$H + H_2 \rightarrow H_2 + H$$

and its isotopic analogs. Its simplicity arises partly from the small number of electrons, which facilitate the construction of an accurate potential surface for the H_3 system, and partly from the lightness of the hydrogen atoms, which limit the accessible product quantum states (channels). Starting with the early efforts of London, Eyring, and Polanyi,[1,2] the $H + H_2$ reaction family has been the focus of extensive theoretical efforts to model reaction dynamics.[3] Today, the H_3 potential surface is the most accurately known for any neutral reactive system,[4] and it is one of the few systems for which the dynamics have been treated quantum mechanically in three dimensions.[5–7] Such rigorous calculations increase in difficulty as the energy of the system exceeds threshold and consequently these have been carried out to date only over a limited range of collision energies. Nevertheless, these results serve as an important test in developing approximate theories of reaction dynamics.[3]

For this fundamental reaction, experimentalists have been hard pressed to keep up with theory. This is a consequence of a number of factors. The $H + H_2$ reaction system has a large activation energy (~ 0.33 eV) requiring the generation of fast H atoms. Moreover, the reaction cross section is small, on the order of 1×10^{-16} cm^2, so that product yields are low. Finally, the reaction product is difficult to detect, especially in a quantum-state-specific manner. Consequently, while state-to-state reaction dynamics have been investigated for a number of chemically interesting systems,[8–10] such studies have only become possible for the $H + H_2$ system within the last year. Two groups have independently reported somewhat similar experiments designed to overcome the above difficulties. Both employed a laser-photolysis method to produce fast H atoms for reaction with D_2 and have utilized sensitive nonlinear spectroscopic techniques to determine quantum state distributions for the HD product. Gerrity and Valentini[11] have used coherent anti-Stokes Raman spectroscopy (CARS) while Rettner, Marinero, and Zare[12] have employed multiphoton ionization (MPI).

We present here a full account of our previous preliminary report and include new results for the HD product in $v = 2, J = 0$–6. A novel laser photolysis MPI time-of-flight instrument is described in some detail and our findings are compared to those of Gerrity and Valentini[11] and to the recent three-dimensional quasiclassical calculations of Blais and Truhlar.[13]

II. EXPERIMENTAL

A. General

In order to study the detailed dynamics of the $H + H_2$ family of reactions, it is necessary to bring together the reagents at sufficiently high collision energies and densities to ensure a measurable product yield. Moreover, these conditions must be compatible with a method for the sensitive quantum-state-specific detection of the reaction products. These requirements place stringent constraints on the design of the experiment. Our basic approach utilizes an effusive flow of a mixture of the reagents, where we take no advantage of the beam directionality other than to create a localized high density. In our scheme, hydrogen atoms are produced in the presence of D_2 by laser photolysis and reaction products are interrogated by a second laser which is fired

[a] Present address: IBM Research Laboratory, San Jose, California 95193.

 0021-9606/84/094142-15$02.10

after a delay that is long enough for some reaction to occur, but prior to any substantial product-state relaxation. This so-called "pump-and-probe" approach is basically a laser version of the classical flash-photolysis method[14] and has previously been successfully employed by a number of workers, particularly in studies of the reaction of excited atoms.[15–18] While this basic scheme permits reagents to be brought together at relatively high densities and under essentially collision-free conditions, in this instance it also provides the necessary means of generating the reagent collision energy. Since the ~0.33 eV activation energy of these reactions corresponds to some 4000 K, such photochemical activation is vital to the success of any mixed-gas approach.

This method of producing fast hydrogen atoms for reactive studies far predates the advent of lasers. More that 35 years ago, Williams and Ogg[19] photolyzed HI with the 253.7 nm line of a mercury lamp and observed greatly enhanced H atom reaction rates. Later studies were concerned with reactions such as D + H_2, CH_4, and C_2H_4[20,21] and H + D_2, CD_4, and C_2D_6.[21] This culminated in the elegant studies of Kuppermann and White[22] who used different photolysis wavelengths to determine the threshold for the reaction D + H_2. The introduction of powerful UV laser sources has brought about a revival of interest in this photolytic production of "hot" hydrogen atoms. While the first laser workers were concerned with energy transfer (T-V) processes.[23–25] Quick and Moore[26] recently reported the first reactive studies.

Let us now consider the "probe" aspects of our pump-and-probe scheme. The quantum-state-specific detection of molecular hydrogen has been demonstrated using MPI[27,28] CARS,[11,26,29–31] and laser-induced fluorescence (LIF),[32,33] as well as high-resolution photoelectron spectroscopy (PES).[34–36] Of these, the MPI and LIF methods offer the highest reported sensitivities, of which we have chosen the MPI approach, while Gerrity and Valentini[11] have successfully employed CARS to detect nascent HD reaction products.

State-specific detection of HD is achieved by resonant two-photon excitation to the double-minimum $E, F\,^1\Sigma_g^+$ state. A subsequent photon is then absorbed to produce HD^+ ions which are sensitively detected. The basic two-photon excitation scheme was first demonstrated by Kligler *et al.*[37] who detected near-infrared emission from the H_2 $E, F\,^1\Sigma_g^+$ to the H_2 $B\,^1\Sigma_u^+$ state, while Marinero *et al.*[27,28] have recently described a more sensitive multiphoton ionization scheme. Figure 1 displays the potential energy curves involved in this process. Note that at the high laser intensities ($\sim 10^9$ W cm^{-2}) required to excite the two-photon step, ionization, caused by absorption of a subsequent photon, competes strongly with and may even dominate over radiative decay.

The sensitivity of the MPI technique depends heavily on the ability to collect ions with close-to-unit efficiency and to employ a charged-particle multiplier to amplify signals. In addition, in these experiments, it is necessary to utilize mass selection of the detected ions to separate them from the large numbers of background ions produced by the high-intensity UV sources used. The operation of an electron multiplier and time-of-flight mass selection both dictate pressures $\lesssim 10^{-5}$ Torr. However, the reaction cross section is so small,[3] $\sim 1\times 10^{-16}$ cm^2, that a detectable product flux demands pressures $\gtrsim$ 10 mTorr. Thus, a differentially pumped system is required, in which reaction products are extracted from a relatively high pressure region into an independently pumped section where the ions are separated according to mass before detection.

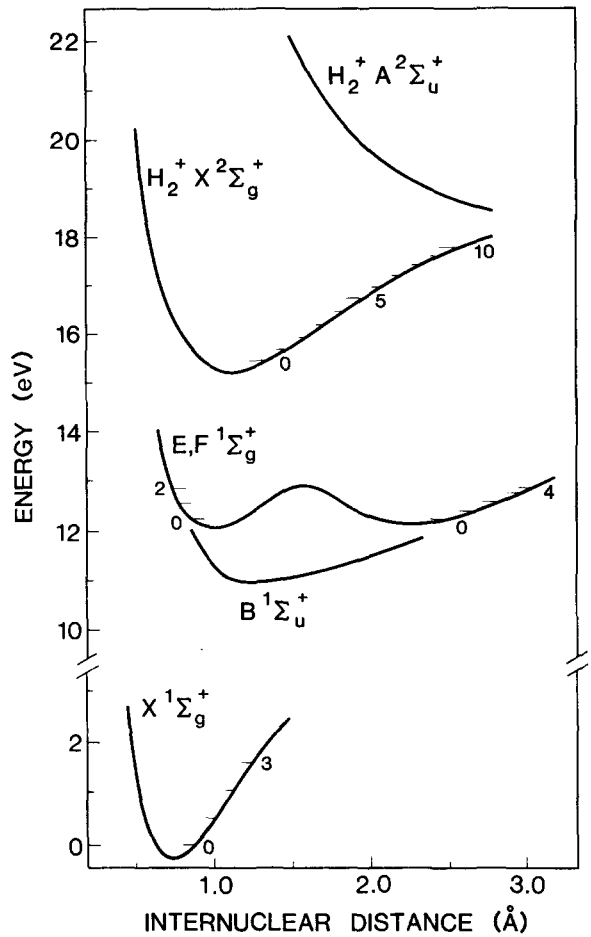

FIG. 1. Relevant potential energy curves involved in the two-photon resonant, three-photon ionization of molecular hydrogen.

Unfortunately, some of the more obvious designs for such an arrangement proved to be unacceptable. Two particular problems deserve mention: (i) since high voltages are required for efficient ion extraction, careful design is required to avoid electrical breakdown; and (ii) since photon energies in excess of 5 eV are needed, care must be taken to prevent spurious ionization arising from the production of photoelectrons by the scattered laser light. Finally, we note that the vacuum system should be kept as clean as possible. This is necessary to minimize the concentration of easily ionized organic contaminants as well as that of molecular hydrogen which emanates from the stainless steel vacuum walls.

B. Detailed description

1. Production of fast H atoms

Fast H atoms are produced by photolyzing hydrogen iodide (HI) using the fourth harmonic of a Nd:YAG laser at 266 nm (Quanta-Ray, DCR-2) operated at 10 Hz. Figure 2

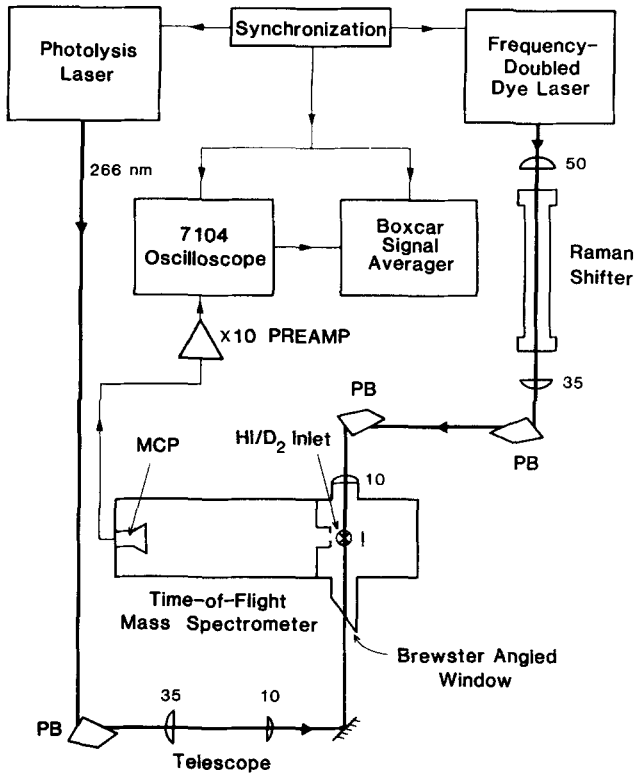

FIG. 2. Experimental setup for product-state distribution measurements of the H + D_2→HD + D reaction. The number by each lens is its focal length in cm; PB = Pellin–Broca prism; and MCP = multichannel plate ion detector.

presents an overview of the experimental layout. A Pellin–Broca suprasil prism isolates the 266 nm output. The resulting pulse (10 mJ, ~5 ns duration) is collimated to a ~2 mm diameter beam using an inverted telescope, consisting of 35 and 10 cm lenses. The beam is then steered through the vacuum chamber using a single kinematically mounted dielectric mirror. The photolysis beam is linearly polarized with its electric vector pointing in the plane of Fig. 2.

Hydrogen iodide was chosen as the source of H atoms as it has the largest photodissociation cross section of any suitable hydride at 266 nm. At this wavelength the photolysis of HI has two channels; H + $I(^2P_{3/2})$ and H + $I(^2P_{1/2})$, which results in a ~2:1 ratio of "fast" to "slow" H atoms.[38–41] These yield CM collision energies with D_2 of 1.30 ± 0.04 eV and 0.55 ± 0.03 eV, respectively, as shown in the Appendix. The HI gas was obtained from Scientific Gas Products and was purified by repeated freeze–pump–thaw cycles to 77 K. This served to remove H_2 gas which is always present in the HI sample.

2. Multiphoton ionization of reaction products

Both reaction products, HD(v,J) and D are detected by three-photon ionization. The probe beam is derived by Raman shifting a YAG-pumped frequency-doubled dye laser (Quanta-Ray, DCR-1A/PDL/WEX system) which is synchronized to the photolysis laser at variable delay by a 50 MHz pulse delay generator (Hewlett–Packard, 8015A). Using a fast biplanar photodiode (ITT, 4115) in combination with a 1 GHz oscilloscope (Tektronix, 7104) we measured a

TABLE I. Vacuum wave numbers (cm^{-1}) of the HD $E, F\,^1\Sigma_g^+ - X\,^1\Sigma_g^+$ transitions[a] utilized to measure ground state populations.

Q	(0,0)	(0,1)	(0,2)	(0,3)
0	99 301.52	95 669.36	92 214.65	88 933.79
1	99 260.12	95 631.81	92 181.08	88 903.92
2	99 177.52	95 556.94	92 113.58	88 843.96
3	99 054.3	95 444.12	92 013.18	88 754.62
4	98 891.7	95 298.0	91 880.83	88 637.01
5	98 690.7	95 115.73	91 717.34	88 491.86
6	98 452.3	94 896.7	91 523.96	88 320.26

[a] The transition frequencies are based on the measurements of G. H. Dieke, Phys. Rev. **50**, 797 (1936) for the HD E, F–B system combined with the measurements of I. Dabrowski and G. Herzberg, Can. J. Phys. **54**, 525 (1976) for the HD B–X system.

temporal jitter of ~ ± 1 ns between the probe and photolysis lasers, over a delay range ~ ± 1 μs. For our typical dye laser energies ~75 mJ in a ~5 ns pulse, we obtain ~15 mJ of frequency-doubled radiation, which upon Raman shifting in a cell of H_2 (7 atm), yields ≳100 μJ for the various anti-Stokes orders.

After recollimation the Raman cell output is dispersed by a Pellin–Broca prism which directs the desired horizontally polarized order into a second (mirror image) prism which deflects it through the reaction chamber (see Fig. 2). An f = 10 cm MgF_2 lens focuses the probe beam to ≳40 μm diameter spot at the center of the reaction zone. The beam propagates counter to the photolysis laser and exits the reaction chamber through a quartz Brewster-angled window after which a small fraction is picked off with a 90° prism and imaged onto a pyroelectric joulemeter (Molectron J3-05) to provide a monitor of the anti-Stokes energy. The back-to-back Pellin Broca arrangement ensures that the direction of the probe beam is independent of wavelength.

The quantum-state-specific detection of HD (v = 0–3, J = 0–6) requires tunable radiation in the 200–226 nm range to excite the Q-branch members of the $E,F\,^1\Sigma_g^+(v=0)$–$X\,^1\Sigma_g^+(v=0$–$3)$ two-photon transitions. Table I lists the frequencies of the Q-branch lines of the (0,0), (0,1), (0,2), and (0,3) bands of this system. Table II describes the excitation scheme employed for each of these bands.

In addition, we detect the D atom product of the reaction, as well as the H-atom reagent, via three-photon ionization resonantly enhanced by their 1s–2s two-photon transitions at 82 281.32 and 82 258.95 cm^{-1}, respectively.[42] Again, details of the excitation scheme are specified in Table II.

3. Detection of ions

As discussed in Sec. II A, in order to optimize both the reaction product yield and the ion collection efficiency, it is necessary to employ a differentially pumped system in which the reaction occurs in a localized region of high reagent density. This is accomplished by introducing the HI and D_2 via a 3 cm long, 0.6 mm diameter fine glass tube which is placed close to the focus of the probe beam and is held on an external translator to permit vertical adjustment with respect to

TABLE II. Detection scheme employed in the MPI detection of HD ($v = 0$–3) and H and D atoms.

	HD $E,F\,^1\Sigma_g^+ - X\,^1\Sigma_g^+$				H,D 1s–2s	
	(0,0)	(0,1)	(0,2)	(0,3)	H	D
Dye laser wavelength (nm)	605–614	565–572	594–600	553–558	609.4	609.2
Anti-Stokes orders of the doubled dye	4th	3rd	3rd	2nd	2nd	2nd
Anti-Stokes peak pulse energy (μJ)	~120	~200	~200	~400	~400	~400
Laser dye[a]	Sulfo-rhodamine 640	Rhodamine 590	Mixture of kiton red + rhodamine 640	Fluorescein 548	Sulforhodamine 640	

[a] Exciton Corp.

the laser beam axis. In practice, the focal point (beam waist) of the desired anti-Stokes order is finely positioned with respect to the tube orifice by adjusting the beam collimation using the 35 cm lens at the exit of the Raman shifter (Fig. 2). This is necessary because of the different degrees of divergence of each anti-Stokes order.

Under typical operating conditions, the probe beam is positioned ~0.75 mm below the tube orifice, where we estimate the densities of D_2 and HI to be ~30 and ~5 mTorr, respectively. These densities are obtained via calibration measurements in which we compare ion signals (H^+ and D_2^+) that result from gases introduced through the glass tube and through a separate needle valve, directly into the chamber. Here the H^+ signal arises when the probe laser, itself, dissociates the HI, and H atoms are ionized as discussed in Sec. II B 2. D_2 is detected in the same manner as for HD. Through this procedure, we estimate the density ratio between the bulk chamber and the relevant position (0.75 mm downstream) in the effusive flow. Thus the pressure at this point is found to be a factor of ~80 times that in the bulk chamber. With the HI/D_2 source on, the reaction chamber pressure rises to $\sim 5\times 10^{-4}$ Torr.

As shown in Fig. 3, the reaction volume and glass delivery tube are located between the acceleration plates of a time-of-flight (TOF) mass spectrometer. Ions are extracted from the reaction chamber via a 1.5 mm wide, 7 mm long

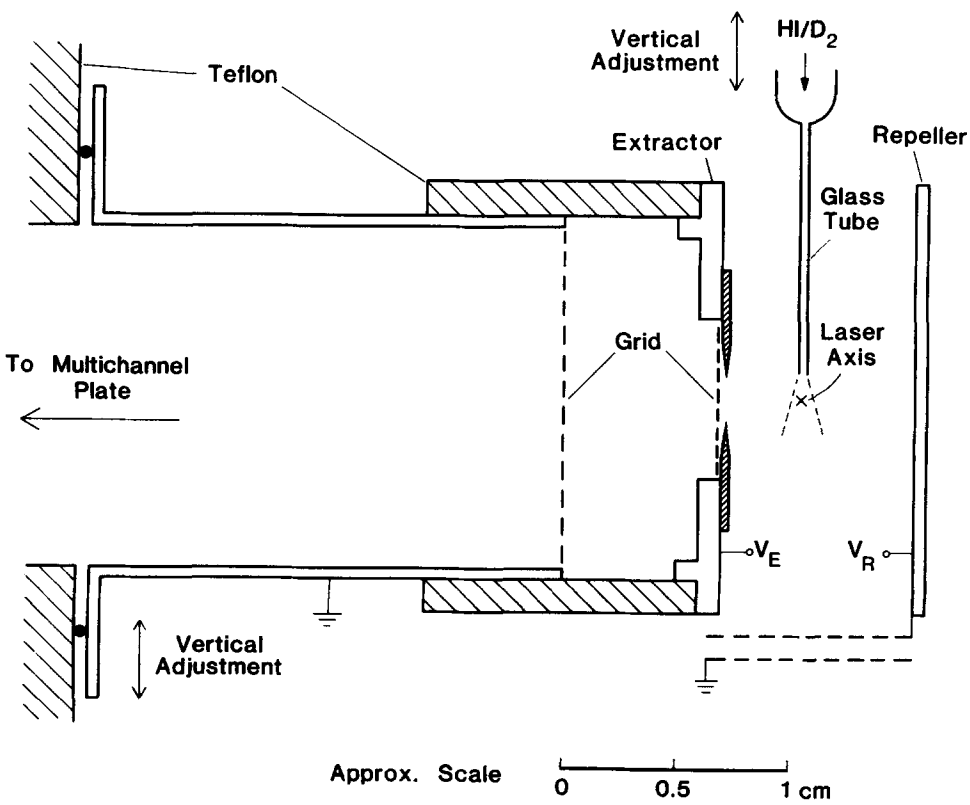

FIG. 3. Detailed drawing of the reaction zone and ion acceleration plates. The glass delivery tube is also shown. Note that both the glass delivery tube and the slit assembly are vertically adjustable using external translators (see the text).

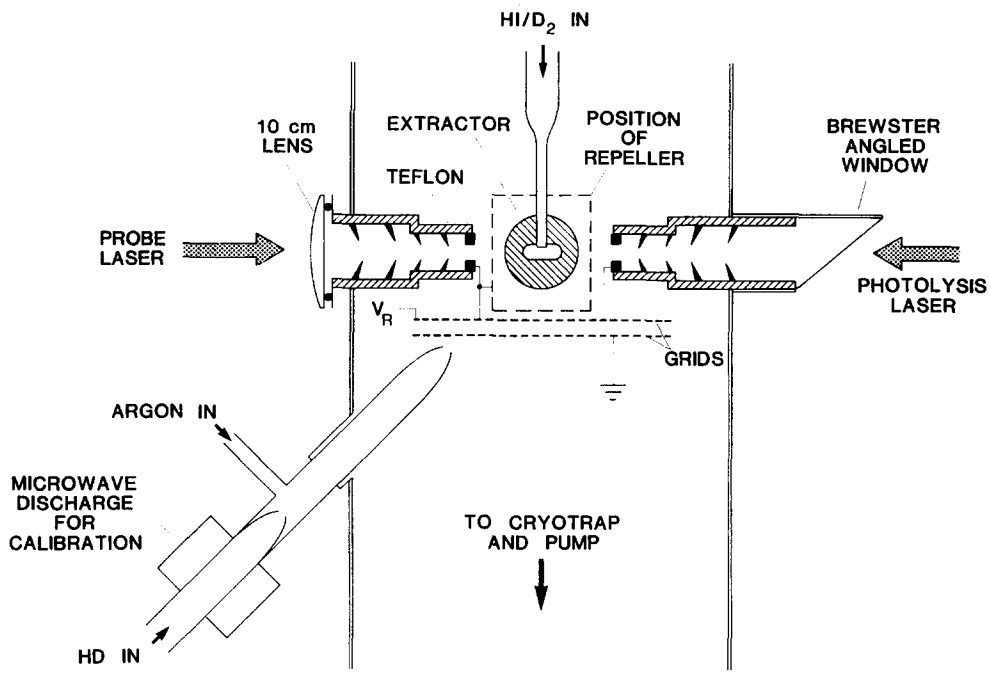

FIG. 4. Cross-sectional view of the reaction chamber and microwave discharge reference source. The horizontal grids screen the ion optics from the discharge tube orifice. The upper grid is held at the same voltage as the repeller plate, while the lower grid is grounded.

aperture (aligned parallel to the laser beam axis) in the extractor electrode. The vertical position of this slit can be adjusted via an external micrometer and is held at a voltage of $\sim +1800$ V, while the repeller plate is biased to $+2400$ V. These two electrodes, as well as additional grids, form part of an assembly which is supported on a fixed Teflon disk, to which a seal is made through a single *O*-ring (see Fig. 3).

It might be anticipated that the introduction of an insulating material, such as the glass delivery tube, between the extractor electrodes would cause severe problems due to the buildup of static charges. This could distort the electric field lines, leading to loss of ion signal and/or a lack of reproducibility. Indeed, we have found exactly such behavior for larger insulators, such as a 6 mm diameter tube. However, the present tube appears not to interfere in this respect. We attribute this difference to the smallness of the current delivery tube.

Electrical breakdown between the repeller plate (held at ~ 2400 V) and the extraction slit assembly is avoided by confining the reaction zone between the acceleration plates of the TOF (Fig. 3). Such a confined high local density also minimizes the attenuation of ion signals due to scattering and ion–molecule reactions.

After crossing the slit assembly the ions experience an acceleration field of ~ 2.5 kV/cm over a ~ 7 mm region between the extraction grid and the first grounded grid of the TOF. A second grounded grid placed 70 cm away from the first one, defines the field-free, ion-drift region. A multichannel plate (MCP) (Galileo FTD 2002) is situated 5 mm behind the second grounded grid and its upper channel plate is held at -2000 V.

4. HD(v = 0–3) and D atom reference source

In order to measure nascent distributions of HD ($v = 0$–$3, J$) as well as the translational energy of the fragments, we incorporated a microwave discharge reference source into the reaction chamber which can provide both D atoms and vibrationally excited HD molecules. This is schematically shown in Fig. 4. The discharge cavity is placed outside the vacuum chamber and the discharge products flow along a ~ 20 cm long passivated[43] Pyrex tube to emerge through a ~ 1 mm diameter orifice placed ~ 3 cm away from the laser axis. The microwave flow tube incorporated an internal nozzle arrangement and a secondary port through which buffer gases could be introduced. The purpose of this feature was to enable us to relax collisionally the rotational populations of vibrationally excited HD in order to calibrate our product distributions against a known Boltzmann distribution.

It may be expected that the rotational temperature of the microwave generated vibrationally excited HD is not necessarily that of the flow-tube walls (essentially at 295 K). Indeed, in the absence of buffer gases the rotational distributions for $v = 1,2$ were found to be in agreement with a Boltzmann distribution at 325 K. The addition of argon cooled this somewhat, reaching ~ 310 K for mixtures containing $\sim 90\%$ argon. The slight differences between the power-corrected discharge signals and those predicted from idealized Boltzmann distributions were interpreted as being due to a small rotational dependence of the transition probabilities. Calibration against discharge signals was always made under identical conditions of laser power and ion optics voltage settings. For the data reported here, we employed calibration factors (phenomenological transition probabilities) obtained from pure HD discharges, but which agreed within experimental uncertainties with those obtained in the presence of argon buffer. For HD($v = 1$) $J = 0$–6, these factors are 1.00, 1.02, 0.89, 0.86, 0.90, 1.00, and 0.92, and for HD($v = 2$) $J = 0$–6, they are 1.00, 1.05, 1.07, 1.14, 1.04, 1.00, and 1.00, respectively. In both cases, uncertainties are $\sim 10\%$ except for the $J = 6$ points, which are accurate to

only ~25%. Notice that these correction factors are all close to unity, a finding that has been reported previously for H_2[27,28] and has been found in detailed calculations of the two-photon line strengths for these same transitions.[44]

Two horizontal grids screened the microwave discharge from the ion optics, as shown in Fig. 4. The one closest to the Pyrex tube orifice was held at ground potential while the upper one was biased to the same voltage as the repeller plate. The microwave discharge proved also to be invaluable in checking the spatial overlap of the photolysis and probe lasers within the reaction volume. This was accomplished in the following manner. The probe laser was tuned to excite a given Q line of the HD E,F–X ($v \geqslant 1$) system and the subsequent ionization of the HD absorber monitored using the oscilloscope. As the ionization of the E,F state is not complete and its lifetime is ~100 ns,[37] it became possible to observe a secondary HD^+ peak when the photolysis laser was sent through the excitation volume some 50 ns after the probe laser. The amplitude of this secondary peak was directly related to the degree of spatial overlap between the two beams.

Finally, notice that optical baffles are employed to reduce the level of scattered light impinging on the ion optics. This is necessary because at the photon energies used here, the radiation can give rise to spurious photoelectron signals. In addition, these baffle arms are terminated with an annular section which is held at the bias potential of the repeller plate in order to minimize the number of charged particles entering the reaction zone.

III. RESULTS

A number of checks were made to ensure that the results reported here refer to the H + D_2 reaction. Signals require the presence of both HI and D_2; in the absence of the photolysis laser no signals corresponding to HD($v \geqslant 1$) or D are observed from the probe laser. Moreover, the magnitude of these signals depends sensitively on the delay between the photolysis and probe pulses, as will be described below. We have also excluded the possibility that we are observing HD($v \geqslant 1$) arising from excitation of HD impurity in the D_2 sample. This might be caused by electron or ion impact or by fast H atom energy transfer. The D_2 sample is initially quite pure (nominally 99.9% D) but operationally we detect (by MPI) ~0.5% HD contamination in the D_2, probably due to wall exchange processes. On replacing the D_2 by "pure" HD(>98%), the HD($v \geqslant 1$) signal increased by less than a factor of 2 indicating that HD excitation contributes <1% to the HD($v \geqslant 1$) signal we observe in the H + D_2 reaction. These findings show that the energy transfer/H atom exchange cross section for the process

$$H + HD(v = 0) \rightarrow H + HD(v \geqslant 1)$$

must be of the same magnitude or smaller than the reaction cross section for H + $D_2 \rightarrow$ HD($v \geqslant 1$) + D. Moreover, we find that the HD($v = 1,J$) distribution from H + HD($v = 0$) yields a distinctly different rotational distribution than that from H + D_2. Finally, we consider the possibility that HD($v \geqslant 1$) might arise from the reaction of D atoms with HI. These D atoms could originate from either the H + D_2 reaction or from the photolysis of DI present in the HI sample. The former process requires a consecutive reaction scheme which might contribute to the HD($v \geqslant 1$) signal at later times but can be ruled out at earlier times from the temporal evolution of the signal reported below. The latter process can also be excluded on the grounds that the HI sample only contains DI at natural abundance (<0.1%), and that, as stated before, the HD($v \geqslant 1$) signals depend on the presence of both HI and D_2.

A. HD(v = 1) Rotational distribution

As mentioned above, the HD^+ ion signals from the HD($v \geqslant 1$) reaction products depend sensitively on the relative delay between the photolysis and probe lasers. When the probe laser *precedes* the photolysis laser, no signals are observed. Signals begin to appear when the two lasers are fired simultaneously and peak at a delay of ~100 ns, as shown in Fig. 5 for the HD($v = 1, J = 2$) product which is obtained at a D_2 density ~10^{15} molecules cm^{-3}.

Under these conditions, for an H atom velocity of 1.8×10^4 m s^{-1}, one hard sphere collision ($\sigma = 4 \times 10^{-16}$ cm^2) requires on average ~1.4 μs, while the reaction of H + D_2 ($\sigma \simeq 1.0 \times 10^{-16}$ cm^2)[3] requires ~5.8 μs. Further, since the photolysis volume has a radius of ~1 mm, a time of $\gtrsim$ 60 ns must pass before the fraction of fast H atoms escaping from this volume becomes appreciable. Consequently, we attribute the initial growth of the signal in Fig. 5 to collisions between fast H atoms and D_2, while at a delay time greater or on the order of 100 ns, this growth is arrested by the escape of the H atoms from the reaction volume.

The ion signals as a function of probe laser wavelength corresponding to the reaction product HD in $v = 1, J = 0$–6 are presented on the left-hand side of Fig. 6. These signals are obtained using a delay time of 62 ns between photolysis and probe pulses. They constitute single scans of the Q members of the HD E,F–X (0,1) band using a total accumulation time of ~60 s for each rotational transition. The HD($v = 1, J = 0$–6) ion signals are recorded with the same signal-recovery gain factors; their excellent signal-to-noise ratios are apparent. For comparison, ion signals correspond-

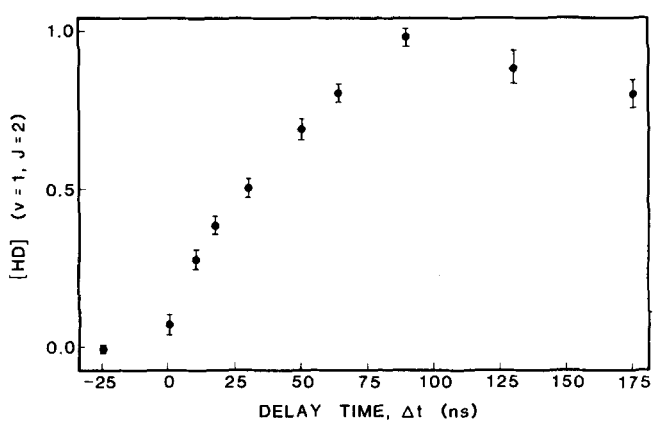

FIG. 5. HD($v = 1, J = 2$) product temporal evolution. The signal growth is displayed as a function of the delay time between photolysis and probe laser pulses. Negative delay implies that the probe laser *precedes* the photolysis source. Error bars represent one standard deviation.

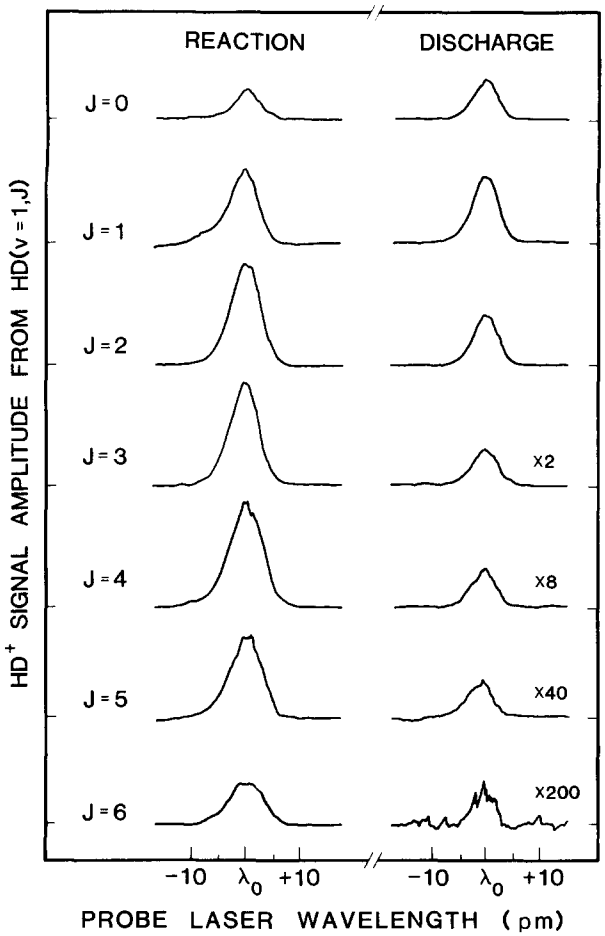

FIG. 6. MPI signals for the HD($v = 1,J = 0$–6) product of the H + D_2 reaction and for HD($v = 1$) generated in the reference microwave discharge. These signals arise from the two-photon Q-branch excitation of the HD $E,F\,^1\Sigma_g^+$–$X\,^1\Sigma_g^+$ (0,1) band. Thus the λ_0 values correspond to one half the transition frequencies listed in Table I, where 1 pm = 10^{-3} nm≃0.23 cm^{-1}. Note the change in signal gain for the discharge data.

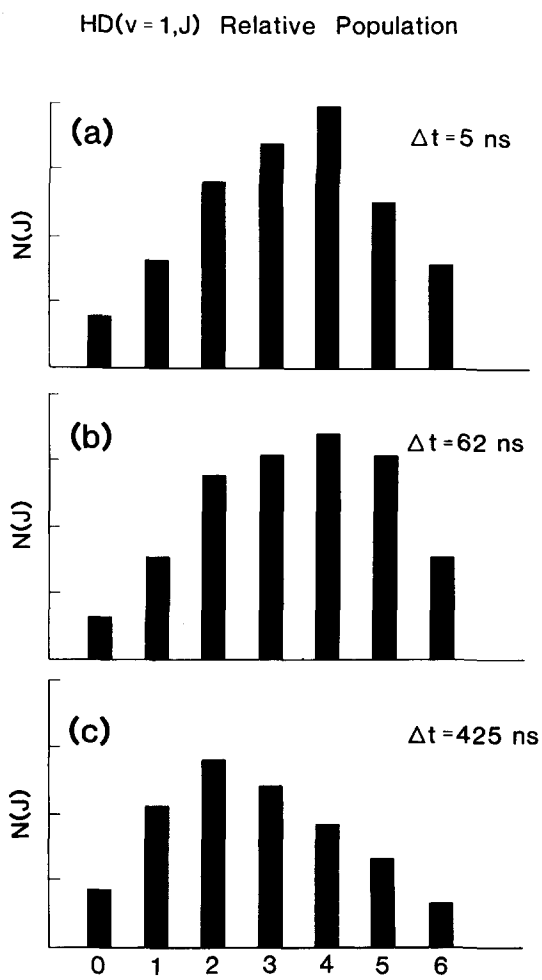

FIG. 7. HD($v = 1$) rotational distributions recorded for different delay times between the photolysis and probe laser pulses. The distributions are normalized to the strongest member of each individual set.

ing to HD in $v = 1$ generated in the microwave discharge are shown on the right-hand side of Fig. 6. It should be noted that the gain factor utilized to record HD($v = 1,J = 6$) from the discharge source is a factor of 200 times greater than that used for HD($v = 1,J = 0$). This is a consequence of the fact that under the conditions of our discharge environment the rotational energy difference of 1756 cm^{-1} between these two levels leads to a population ratio of ~180:1 for a rotational temperature of 325 K. Thus it is evident that the HD($v = 1$) reaction product is rotationally hot.

In addition, even though the line profiles are dominated by the laser bandwidth, careful inspection shows that the line shapes of the HD($v = 1$) reaction products are significantly broader (⩾20%), indicating that these species are also translationally hot. A simple Doppler analysis, assuming a Gaussian spread of HD laboratory velocities and taking account of the laser bandwidth yields an estimate of the nascent HD laboratory velocity component parallel to the probe beam direction. We obtain a mean velocity of ~3800 ± 600 m s^{-1}, measured at a delay of ~60 ns. It is emphasized however, that the HD velocity profile may not be Gaussian and that this measurement is highly sensitive to velocity-changing collisions. Thus the quoted value should be taken only as a guide to the actual HD velocity.

The effect of collisions on the nascent rotational distribution of HD($v = 1$) is investigated by recording ion spectra, such as the ones shown in Fig. 6, at several delay times. Using our calibration procedure and power corrections of the ion signals (see Sec. II B 4), we are able to obtain relative rotational populations as a function of delay. Figure 7 illustrates these results in which the HD($v = 1,J$) distributions are given for delay times of 5, 62, and 425 ns. These data represent the average value of our power-normalized ion signals. The full data set, including uncertainty estimates are listed in Table III. When the error limits of the data are considered, we find that the rotational distributions for delays of 5 and 62 ns are essentially the same. Consequently, we conclude that our experimental conditions may be considered "collision free," at least up to delay times ~60 ns, i.e., collisions do not serve appreciably to slow down the fast H atom reagent or to rotationally relax the HD($v = 1$) product on this time scale.

In contrast, the distribution obtained at 425 ns delay [Fig. 7(c)] is clearly rotationally colder. Furthermore, Doppler width measurements for this distribution indicate

TABLE III. Rotational distributions for HD($v = 1$) ($\Delta t = 5$, 62, and 425 ns) and HD($v = 2$) ($\Delta t = 65$ ns) normalized to HD($v = 1$, $J = 4$) at $\Delta t = 62$ ns. The entries are power-normalized peak heights.

	HD($v = 1$)			HD($v = 2$)
J	$\Delta t = 5$ ns	$\Delta t = 62$ ns	$\Delta t = 425$ ns	$\Delta t = 65$ ns
0	6.9 ± 0.9[a]	19.0 ± 1.5	18.8 ± 1.1	6.0 ± 1.0[b]
1	13.9 ± 1.4	46.3 ± 1.7	46.5 ± 4.1	22.0 ± 1.5
2	23.6 ± 1.7	83.0 ± 4.2	61.1 ± 2.9	26.1 ± 2.4
3	27.9 ± 1.5	90.1 ± 4.5	52.6 ± 4.2	23.3 ± 2.3
4	33.3 ± 2.9	100.0 ± 3.6	41.2 ± 3.8	17.5 ± 3.2
5	20.7 ± 2.6	80.1 ± 8.0	29.3 ± 6.6	13.3 ± 2.2
6	13.2 ± 4.1	46.3 ± 13.2	14.6 ± 5.0	3.9 ± 1.4

[a] The uncertainty ranges quoted represent the margins required to encompass all data points and include due allowance for calibration errors. These margins are considered to be approximately equal to one standard deviation.

[b] These have been normalized to the HD($v = 1$), $\Delta t = 62$ ns data using Eq. (1). The quoted error bars refer only to accuracy within the HD($v = 2$) distribution. Relative to the HD($v = 1$) distribution there is an additional uncertainty of about $\pm 40\%$.

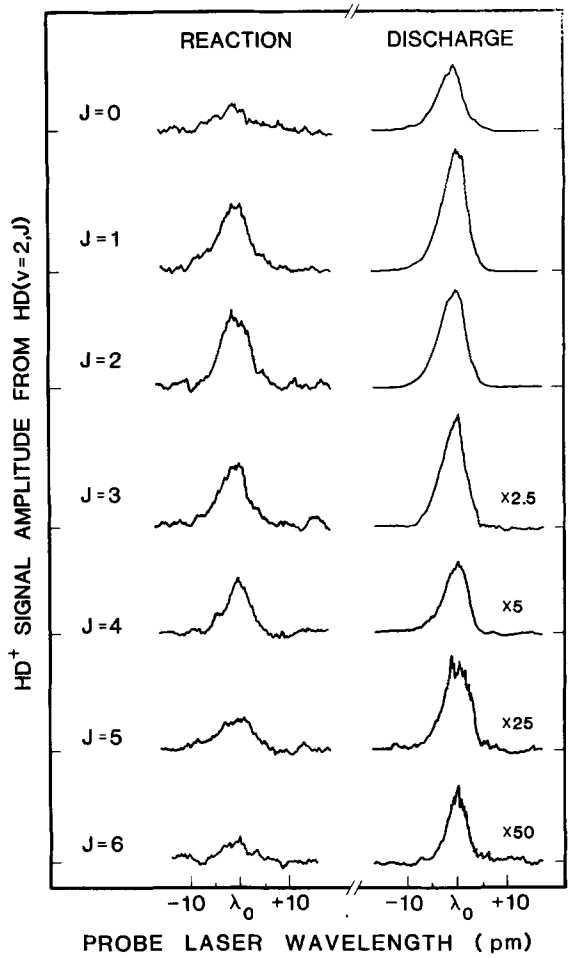

FIG. 8. MPI signals for the HD($v = 2, J = 0$–6) product of the H + D$_2$ reaction and for HD($v = 2$) generated in the reference microwave discharge. These signals arise from the two-photon Q-branch excitation of the HD $E,F\,^1\Sigma_g^+ - X\,^1\Sigma_g^+$ (0,2) band. Thus the λ_0 values correspond to one-half the transition frequencies listed in Table I, where 1 pm $= 10^{-3}$ nm$\simeq$0.21 cm^{-1}. Note the change in signal gain for the discharge data.

that the translational velocity at this delay time is also appreciably lower, approximating thermal values.

We have chosen throughout this work to utilize ion signal heights to derive rotational populations. We find that the peak heights increase linearly as the HD concentration is increased up to an HD pressure $\sim 5 \times 10^{-5}$ Torr. For larger HD concentrations, saturation and space-change effects destroy this linearity. We also note that the same linear response is observed for HD pressures up to $\sim 5 \times 10^{-5}$ Torr mixed with other reagent gases up to total pressures of ~ 100 mTorr. It is recognized that in principle the *area* of the ion signals should be employed for the extraction of relative populations, to allow for possible variation in the linewidths due to different degrees of Doppler broadening. However, because our line profiles are dominated by the laser bandwidth, the variation of linewidth with rotational level is found to be considerably less than variation due to the noise present in the data.

B. HD(v = 2) rotational distribution

Signals for HD($v = 2$) are smaller than for HD($v = 1$). Therefore all HD($v = 2$) product measurements are carried out at delay times of ~ 60 ns since the signal at this delay is larger than at earlier times while they are still expected to be free of significant collisional relaxation effects. Figure 8 presents the counterpart of Fig. 6 for HD($v = 2$). The signal-to-noise ratio is clearly less than for the HD($v = 1$) reaction product. The detection of the higher J members is facilitated in this case compared to that for HD($v = 1$) by the form of the probe-laser power curve. Once again the line profiles of the HD($v = 2$) reaction products exceeds that of the discharge and are approximately the same as those for the HD($v = 1$) products.

Relative rotational populations are presented in Fig. 9 for HD($v = 2, J$) and compared to those for HD($v = 1, J$) for the same time delay (~ 60 ns). Here each distribution is normalized to the most populated rotational level, and not to each other. Clearly the rotational distributions for the two vibrational levels are markedly different, the HD($v = 1, J$) distribution peaking at $J = 4$, while the HD($v = 2, J$) distribution peaks at $J = 2$.

In order to compare the populations of HD products formed in $v = 1$ and $v = 2$, we have measured the absolute ion signals for the $Q(2)$ and $Q(3)$ transition of the (0,1) and (0,2) bands of the E,F–X system. This was done employing essentially the same experimental conditions except for different probe laser powers. Since we do not have a suitable calibration reference for vibrational populations, the determination of the HD($v = 1$):HD($v = 2$) population ratio requires a knowledge of the signal power dependence as well as the relevant multiphoton line strengths. For anti-Stokes energies $\lesssim 200$ μJ, the $Q(2)$ and $Q(3)$ lines were found to vary as I^n, where $n = 2.4 \pm 0.2$, for the (0,1) band, and $n = 2.2 \pm 0.2$ for the (0,2) band. The transition probabilities for two-photon resonant three-photon ionization are presently unknown for this system. However, an estimate can be made if we assume that the multiphoton ionization process has the same probability as the two-photon transitions to the E,F state. Since ionization proceeds through $v = 0$ of the E,F state in both cases, this assumption is equivalent to assuming

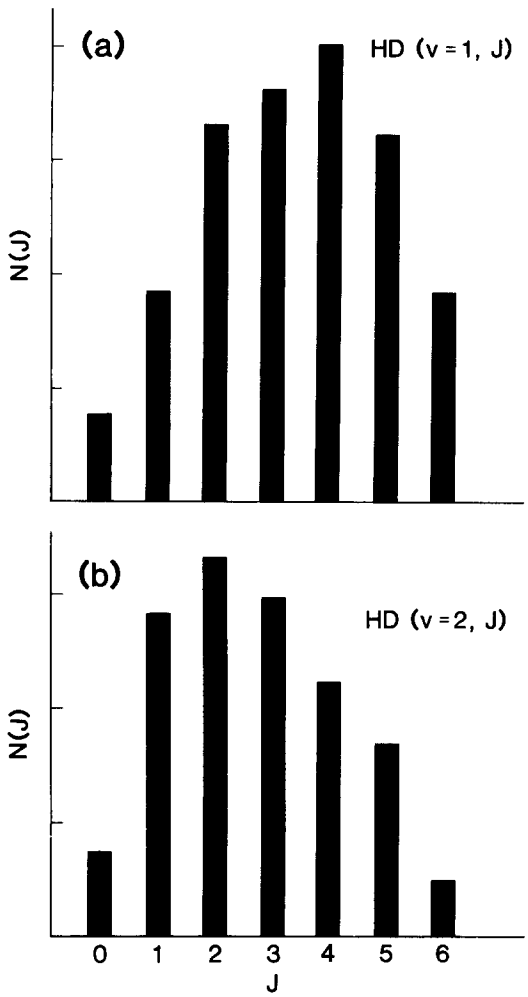

FIG. 9. Rotational distribution of (a) HD($v = 1$) and (b) HD($v = 2$) obtained for a delay time of ~60 ns. The distributions are relative (see the text) and clearly show that the maximum of each distribution occurs at a different rotational level.

that the $\sim 1700\ cm^{-1}$ difference in the energies of the final (ionizing) photons, is unimportant. This is supported somewhat by the fact that the two transitions exhibit similar power dependences. The order of these power dependences are expected to be between 2.0 (for saturation of the final absorption step) and 3.0, when this step is only weakly pumped. Thus the similar power dependences imply similar cross sections for the absorption of the third photon. However, this premise has not been tested in detail and therefore deductions based on it must be considered somewhat tentative.

Two-photon transition probabilities have been provided for us by Huo,[44] who finds that the transition probabilities of the $Q(2)$ and $Q(3)$ lines of the (0,2) band are a factor of 1.28 ± 0.18 times stronger than for $Q(2)$ and $Q(3)$ of the (0,1) band. Thus we obtain from our data the population ratios

$$\frac{[HD(v=1,J=2)]}{[HD(v=2,J=2)]} = 2.9 \pm 1.1 \quad (1a)$$

and

$$\frac{[HD(v=1,J=3)]}{[HD(v=2,J=3)]} = 4.2 \pm 1.7\,, \quad (1b)$$

where uncertainties reflect only the inaccuracies involved in measurements and in the two-photon transition probabilities, no allowance being made for possible errors arising from varying absorption efficiencies for the third photon.

C. HD(v = 0) rotational distribution

Although we have detected the HD($v = 0$) product in $J = 0$ to 6, it was not possible to extract a rotational distribution in this case. Here the ~0.5% HD impurity in the D_2 sample produced a background signal, introducing a large uncertainty in the estimation of those rotational levels that are strongly populated at room temperature. Furthermore, it was found that the firing of the photolysis laser can slightly change (~10%) the overall detection efficiency, thereby somewhat compromising results obtained by a simple subtraction of the HD($v = 0, J$) signals, particularly for $J = 0$ to 3 which have relatively large thermal populations. In the absence of a background contribution from HD impurity, this interference is not apparent, but simply serves to slightly (and consistently) change the detection efficiency, which is always optimized by adjustment of voltages and the slit position prior to measurement. In effect, the photolysis laser slightly changes the optimum geometry for ion detection. We believe that this phenomenon in no way alters any of the reported distributions, for which there is no background HD interference. We note that this small change in detection efficiency responds with a time constant of several seconds and may arise from surface charge buildup, following the introduction of the intense UV photolysis source. Although measurements are possible for $J > 6$, these have not been carried out owing to the lack of a suitable reference source.

In the case of $J = 4$, 5, and 6, the residual background signal amounts to 39%, 21%, and 8%, respectively, of the nascent signal amplitude. An absolute comparison of the signal levels of HD products in $v = 0$ and $v = 1$ was not attempted because of the aforementioned interference. However, a relative comparison of the power-normalized signals for $J = 6$ of HD($v = 0$) to that of HD($v = 1$) yields a ratio of ~3.

For the normalized rotational distribution $J = 4$–6 of HD($v = 0$), we note that $J = 6$ is substantially more populated than in the case of $v = 1$ or 2. The ratio of the relative populations of $J = 5$ to $J = 6$ for HD($v = 0$) is measured as 1.3 ± 0.3, compared to ratios of 1.8 ± 0.5 and 3.4 ± 1.3 for HD($v = 1$) and HD($v = 2$), respectively, for a time delay of $\Delta t \sim 60$ ns. This indicates that the shape of the rotational distribution for HD($v = 0$) around $J = 5,6$ may fall off less rapidly than for the other vibrational levels studied. Finally, we believe that by reducing the HD impurity level and/or by eliminating or fully quantifying the interference effect, it will be possible to extract a distribution for HD($v = 0$, $J = 0$–6).

D. HD(v = 3)

A search was conducted in order to detect HD reaction products in $v = 3$. As indicated in Table II, the detection scheme utilized for two-photon excitation, involves the second anti-Stokes of frequency doubled Fluorescein 548 with an energy of ~450 μJ. This pump power increment can be expected to enhance the detection sensitivity of our system by a factor of 6–11 over that obtained for the detection of

HD($v = 2$). Moreover, the two-photon transition probabilities for the (0,2) and (0,3) bands of the E,F–X system are calculated to be in the ratio of 1.4 ± 0.2.[44]

In spite of the enhanced sensitivity and comparable two-photon transition probabilities, the search revealed *no* evidence for product HD in $v = 3$ within our signal-to-noise limitations. In contrast, HD($v = 3$) generated in the microwave discharge was readily detected. A measurement of the signal amplitudes for product HD in $v = 2$ under identical experimental conditions to those utilized in our search for HD($v = 3$), permits us to set an upper bound on the reaction yield for HD in $v = 3$. We find

$$\frac{[\mathrm{HD}(v=2,J=3)]}{[\mathrm{HD}(v=3,J=0)]} \geqslant 18 . \tag{2}$$

E. Deuterium atom reaction product

The D-atom product evolution from the H + D_2 reaction is shown in Fig. 10. The D-atom signal amplitude is plotted vs the delay between the photolysis and probe lasers. When the probe laser precedes the photolysis laser, no D^+ signals are observed. A measurable product signal is obtained at zero delay and subsequently grows to a maximum for a delay time of ~75 ns. Further increase of this delay results in reduction of the D-atom product signal amplitude. Based on the same considerations outlined in Sec. III A, we attribute the initial growth to collisions between fast H atoms and D_2 which generate nascent D atoms. The decay portion of the signal evolution is due to the escape of both fast H atoms and the D-atom products from the photolysis volume.

Figure 11 presents the D-atom Doppler profile from the H + D_2 reaction for a delay time of 8 ns. This is compared in Fig. 11 with the corresponding profile for thermal D atoms generated in the microwave discharge. It is evident from this figure that the nascent D atoms possess a high degree of translational energy.

Using the thermal D-atom result to correct for laser bandwidth, we can obtain a rough estimate of the mean D atom laboratory velocity parallel to the probe laser direction. Assuming that the velocity distribution is Gaussian, we obtain a mean velocity of 8400 ± 800 m s^{-1}. From similar measurements we find that after ~250 ns, this distribution is somewhat colder, i.e., 2900 ± 300 m s^{-1}, but still somewhat hotter than for thermal (300 K) D atoms for which we obtain a mean velocity $\simeq 1900 \pm 200$ m s^{-1}.

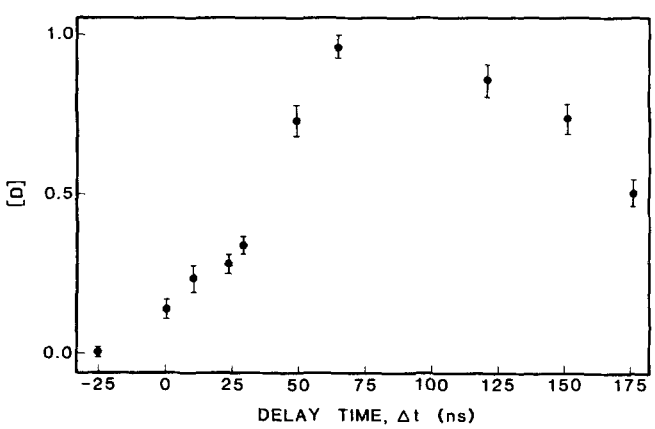

FIG. 10. Deuterium atom product evolution from the H + D_2 reaction as a function of the delay between the photolysis and probe laser pulses. Error bars represent one standard deviation.

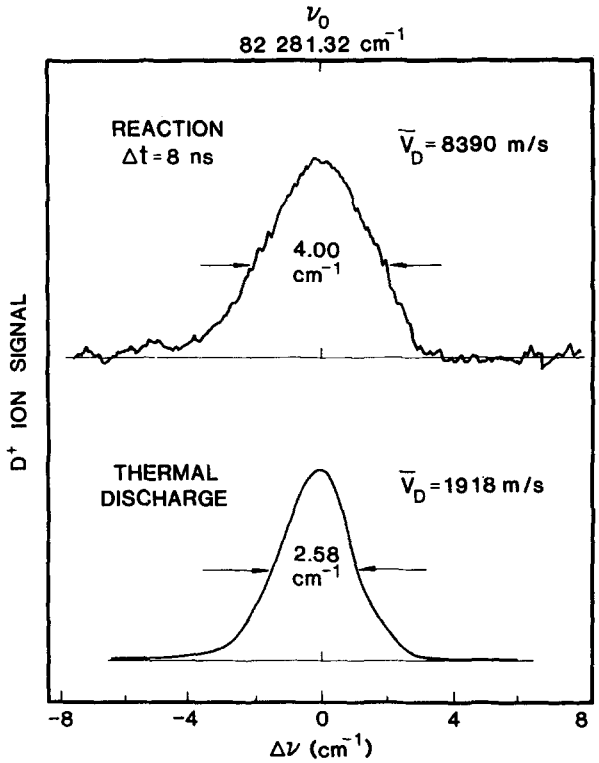

FIG. 11. Deuterium atom line shapes. The upper trace corresponds to the nascent D atom product from H + D_2; the lower trace is for thermal D atoms produced in the microwave discharge. The reaction product exhibits marked Dopper broadening.

F. Reaction cross section

An estimate for the reaction cross section $\sigma(v,J)$ into a given product state can be made using the relationship

$$\frac{d[\mathrm{HD}(v,J)]}{dt} = \sigma(v,J) V_{\mathrm{rel}} [\mathrm{H}][\mathrm{D}_2] , \tag{3}$$

where V_{rel} is the reagent CM relative velocity. This requires a knowledge of (i) the absolute rate of HD product appearance, (ii) the initial density and velocity of the fast H atom reagent, and (iii) the density of the D_2 reagent. Condition (i) may be satisfied by calibration, for example by comparing HD^+ ion signals from the reaction to those from a known density of HD present in the D_2 sample. The velocity of H atom reagents is known here, and H-atom densities can be estimated from a knowledge of the initial HI density, the laser energy, the diameter of the photolysis beam, and the dissociation cross section.[38] Thus condition (ii) can also be met. Finally, the density of D_2 reagent can be obtained by calibration. Unfortunately careful measurements have not yet been made simultaneously on all of these quantities. Nevertheless, we are able to estimate all of these factors to better than an order of magnitude, which provides a crude estimate of the reaction cross section. We estimate the rate of appearance of HD($v = 0, J = 4$) product by comparing the density of nascent HD in this state after 60 ns to the density present

from the HD impurity. This leads to a rate of appearance for HD($v=0$, $J=4$) of $\sim 1\times 10^{18}$ molecules s^{-1}. The D_2 and HI densities are $\sim 1\times 10^{15}$ and $\sim 2\times 10^{14}$ cm^{-3}, respectively, and there is approximately 10% dissociation, 60% of which is to produce the fast H atoms.[38–41] This leads to $[H]\sim 1\times 10^{13}$ cm^{-3}, while $V_{rel}\sim 1.8\times 10^{6}$ cm s^{-1}. Thus we find that

$$\sigma(v=0,\ J=4)\cong 5^{+5}_{-4}\times 10^{-17}\ \text{cm}^2, \tag{4}$$

where the error margins represent roughly one standard deviation. Recalling that there is a $\sim$2:1 ratio of 1.3–0.55 eV relative collision energies and using Blais and Truhlar's estimate[13] that the former contributes about twice the latter to the formation of HD($v=0$,$J=4$), the corrected 1.3 eV partial cross section is approximately 75% of that shown in Eq. (4). To obtain a total reaction cross section requires a knowledge of the partitioning into the HD($v=0$,$J=4$) product channel. Blais and Truhlar[13] calculate that $\sim$5% of the HD reaction product is produced in this state for 1.3 eV collisions. Using this value yields an estimate of

$$\sigma_{\text{TOTAL}}=\sum_{v,J}\sigma(v,J)=7.5^{+7.5}_{-6}\times 10^{-16}\ \text{cm}^2 \tag{5}$$

for the reaction of H + D_2 at a collision energy of $\sim$1.3 eV. This estimate comes surprisingly close to encompassing the total cross section obtained by Blais and Truhlar,[13] $1.13\pm 0.02\times 10^{-16}$ cm^2. We do not consider the difference to be statistically significant.

IV. DISCUSSION

A. Energetics

The photolysis of HI at 266 nm proceeds through two channels, leading to H + I($^2P_{3/2}$) and H + I($^2P_{1/2}$), which result in H atom velocities of 17 660 and 11 460 m s^{-1} in the ratio of $\sim$2:1,[38–41] corresponding to center-of-mass collision energies with D_2 of 1.30 ± 0.04 and 0.55 ± 0.03 eV, respectively (see the Appendix). However, the cross section for production of HD($v\geqslant 1$) is expected to be much smaller at the lower collision energy.[13,45] Indeed, in a quasiclassical trajectory study, Blais and Truhlar[13] found that for this combination of reagents, the contribution from the $\sim$0.55 eV collisions to HD($v=0$,$J\geqslant 5$) is at most 18%, and usually much less. Thus we conclude that the results presented pertain almost exclusively to a collision energy of 1.30 eV. Since we are dealing with a nearly thermoneutral system ($\Delta H=+0.04$ eV), the reaction dynamics serve only to channel the collision energy into the different degrees of freedom of the product. Thus control of the collision energy is of fundamental importance here; any uncertainty in the collision energy is qualitatively equivalent to an uncertainty in the product-state distribution. This emphasizes the value of the pump-and-probe technique employed, since other (e.g., beam) techniques might produce wide distributions of collision energies, obscuring comparison with theoretical predictions.

Simultaneous conservation of energy and of linear momentum requires that for an initial H atom velocity of 17 660 m s^{-1}, HD($v=1$,$J=0$) and HD($v=2$,$J=0$) products must have laboratory velocities in the ranges -1000 to 8100 and 300 to 6700 m s^{-1}, respectively, where the lower velocity limit corresponds to backward scattering in the center-of-mass frame and the upper limit to forward scattering. Here the negative sign in front of the HD($v=1$,$J=0$) backscattering velocity indicates that the HD is backscattered *in the laboratory* with respect to the direction of the H atom reagent velocity. Note that for higher J levels, slightly lower velocities should result; HD($v=1$, $J=9$) e.g., would have similar velocities to the nearly isoenergetic HD($v=2$, $J=0$) state.

The D atom product will take laboratory velocities in the range 12 100 to -5100 m s^{-1}, for backward and forward CM scattering, when the corresponding product is HD($v=0$,$J=0$). For HD($v=1$,$J=0$) and HD($v=2$,$J=0$) this range becomes 10 400 to -3400 and 8300 to -1300 m s^{-1}, respectively. Again, negative values correspond to laboratory backscattering. Since both theory[13] and experiment[11] indicate that HD($v=0$) is the dominant product, the effective range of D atom velocities may well be closest to the first of these, i.e., $\sim$12 100 to -5100 m s^{-1}.

This overall picture is also supported by Figs. 5 and 10. In Fig. 5 it is seen that the falloff in the HD($v=1$,$J=2$) signal only becomes appreciable for times $\gtrsim$ 100 ns, while in Fig. 10 it is apparent that the D atoms fly out more rapidly, as a consequence of their higher velocities.

In principle, careful analyses of Doppler profiles could provide insight into the angular distribution of scattered products. We estimated nascent D and HD($v=1$) velocities of $\sim$8400 and 3800 m s^{-1}, respectively. These appear closest to the "backscattering" limits, as might be expected for a reaction cross section of only $\sim 10^{-16}$ cm^2.[3,13]

B. HD product state distributions

With velocities of $\lesssim$ 8000 m s^{-1}, the HD($v\geqslant 1$) product molecules will move less than 0.5 mm in 60 ns, or no more than a quarter of the diameter of the photolysis volume. Thus when we probe at such a delay, we are essentially detecting the density corresponding to the time-integrated flux of reaction products into each product quantum state. Notice that provided the probe laser is approximately centered and is fully contained within the photolysis volume, its actual diameter does not affect this argument. Hence, we conclude that *the measured product quantum-state distributions correspond directly to the relative rates of reaction into these states*. At longer times, where significant "fly-out" can occur, it would be necessary to correct the observed distribution to allow for the differing product-state velocities.

1. Comparison with quasiclassical calculations

Figure 12 shows the HD($v=1$ and $v=2$) rotational state distributions for $\Delta t=\sim$60 ns given in Table III. Here the HD($v=2$) data has been normalized with respect to that for HD($v=1$) using the average of the measured ratios for the $J=2$ and $J=3$ populations [see Eq. (1)]. In keeping with the uncertainties involved in these determinations, the absolute position of the HD($v=2$) points relative to HD($v=1$) is

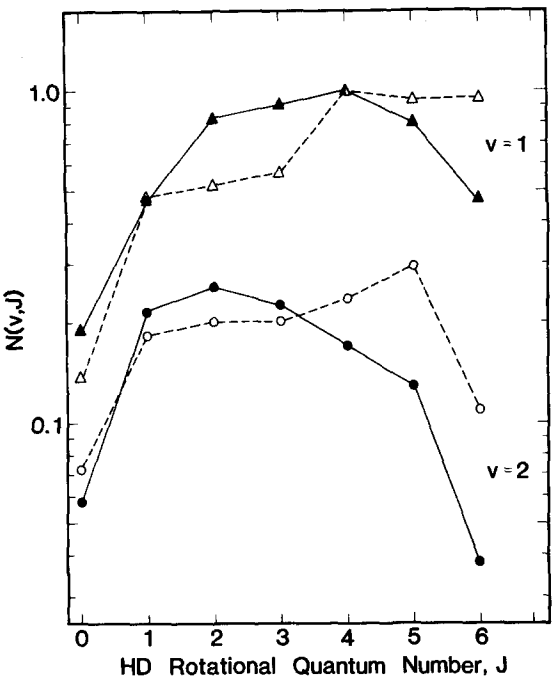

FIG. 12. HD($v = 1$ and $v = 2$) rotational distributions. The solid line and symbols refer to this work while the dashed line and open symbols show the results of the quasiclassical trajectory studies of Blais and Truhlar (Ref. 13).

only considered accurate to within about $\pm$ 40%, whereas within a given vibrational state, uncertainties of $\leqslant \pm$ 15% apply for each point, except for the $J = 6$ data which, due to larger calibration errors, are considered accurate to $\pm$ 30% (see Table III).

Also shown in Fig. 12 are the results of the three-dimensional quasiclassical trajectory studies of Blais and Truhlar.[13] These relative reaction rates have estimated errors in the range $\pm$ 15%–40%, being most accurate for the higher rates. Allowing for the uncertainties associated with the two distributions, the overall agreement between theory and experiment is striking. In particular, both sets of data peak at $J = 4$ for HD($v = 1$) and indicate that HD($v = 1, J = 0$) is formed at a slower rate than HD($v = 2, J = 2$). However, it is also clear that the experimental results differ from the theoretical calculations at high J, indicating a lower degree of rotational excitation than predicted.

We believe that this discrepancy lies outside of the combined uncertainties. The origin of this disagreement is presently unknown but may reflect either the inaccuracy in the potential energy surface, the breakdown of a quasiclassical treatment of the dynamics, or the presence of an undetected systematic error in this work. While the H_3 potential surface has been determined to "chemical accuracy," i.e., the calculated points are thought to lie within 0.1 kcal/mol of the Born–Oppenheimer limit, the overall surface may not be so accurate because (1) calculations were carried out only for a limited range of nuclear configurations and (2) the number of points above 1 eV are few. We also do not understand the differences between quantum and quasiclassical dynamics at these collision energies. Finally, we are aware that our experimental procedure may contain hidden systematic errors that we have not yet uncovered.

2. Surprisal analysis

A number of theoretical studies on the reaction of H with H_2 have found that the H_2 product rotational distributions yield linear surprisals,[5,46–51] or, more loosely speaking, appear "temperature-like." These include two independent 3 D quantum calculations.[5,46,47] Although this work strictly applies to the $H_2(v = 0)$ product of the $H + H_2$ reaction, these results suggested that a similar surprisal analysis might prove useful for our data. This is particularly so since Wyatt[46] obtained a linear surprisal for a total energy as high as 0.8 eV, while Schatz and Kuppermann[5] found linear surprisals for a number of different energies up to 0.7 eV.

The surprisal I for a given product quantum state is defined as[52]

$$I(v,J) = -\ln[P(v,J)/P^0(v,J;E)], \tag{6}$$

where $P(v,J)$ is the observed probability of accessing the (v,J) level and $P^0(v,J;E)$ is the *prior* or statistically most likely probability for a *total* energy E. It can be shown that for the single constraint of conservation of energy,

$$P^0(v,J;E) \propto (2J+1)(\rho_{\text{trans}}) \propto (E - E_v - E_J)^{1/2}, \tag{7}$$

where E_v and E_J are the vibrational and rotational energies of the product. This is calculated for each v,J product level, taking E as 1.51 eV. Here E includes the D_2 reagent zero-point vibrational energy[53] (0.19 eV) and the average rotational energy (0.025 eV), taken for a Boltzmann distribution at 300 K. The HD(v,J) energy levels are obtained from Dabrowski and Herzberg[54] and include the HD zero-point vibrational energy (0.23 eV).

Figure 13 shows the resulting surprisals plotted against the fraction of energy appearing as rotation, $g_R = E_J/(E - E_v)$, for HD($v = 1$), Fig. 13(a), and HD($v = 2$), Fig. 13(b). It is apparent that both give reasona-

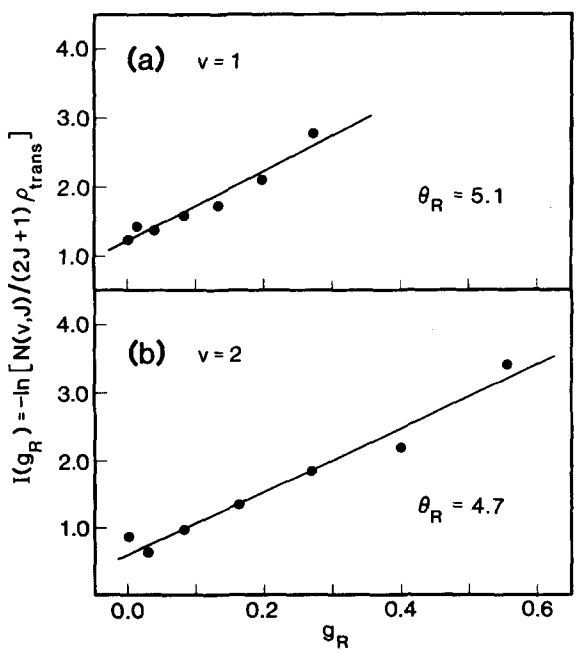

FIG. 13. Rotational surprisal plots for (a) HD($v = 1$) and (b) HD($v = 2$).

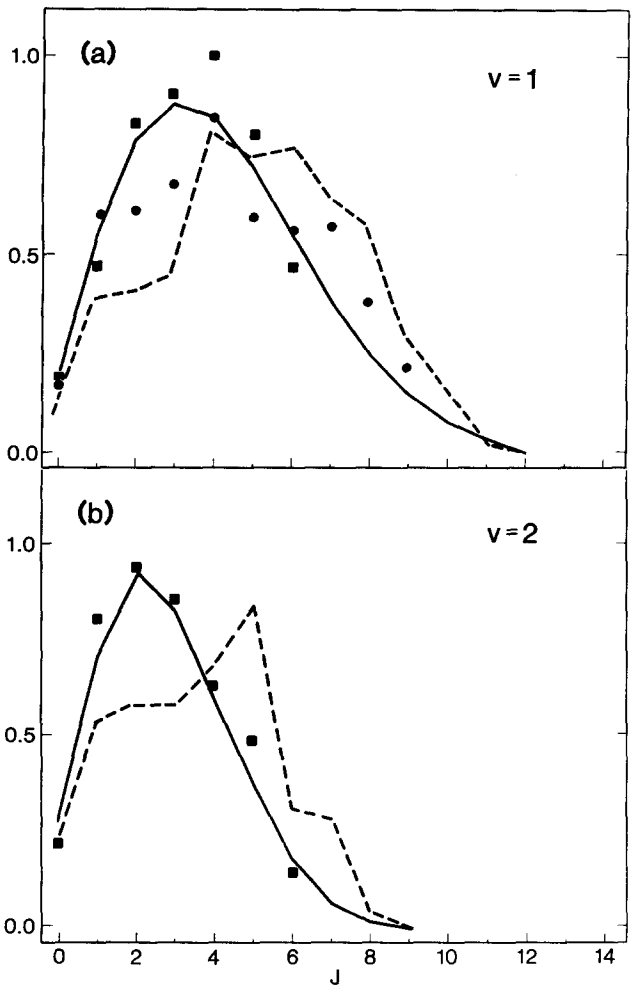

FIG. 14. HD product rotational distributions for (a) $v = 1$ and (b) $v = 2$. The solid curve shows the result of inverting the surprisal procedure using in (a) $\theta_R = 5.09$ for HD($v = 1$) and in (b) $\theta_R = 4.67$ for HD($v = 2$). The dashed curve corresponds to the results of Blais and Truhlar (Ref. 13) while the solid circles indicate the data of Gerrity and Valentini (Ref. 11). Our data points are shown as solid squares.

ble straight lines, with least-squares correlation coefficients of 0.969($v = 1$) and 0.982($v = 2$). This is in keeping with the previous theoretical findings. Moreover, the *slopes* of the two plots are found to be remarkably similar, $dI/dg_R = \theta_R = 5.09$ for $v = 1$ and 4.67 for $v = 2$. We note that simple Boltzmann plots of $\ln[P(v,J)/(2J+1)]$ vs E_J also give reasonable straight lines, corresponding to "temperatures" of 1620 K for HD($v = 1$) and 810 K for HD($v = 2$).

The real value of any surprisal analysis is that it permits energy distributions to be expressed with a minimum of parameters[52] and allows tentative extrapolation of data to include quantum levels not observed. The solid line in Fig. 14(a) displays the idealized quantum state distributions obtained for HD($v = 1$) by inverting the surprisal procedure, assuming linear surprisals with the above-mentioned slopes. Similarly Fig. 14(b) shows the corresponding result for HD($v = 2$). In both cases, the actual experimental points are shown as well as the trajectory results of Blais and Truhlar,[13] which have been normalized such that $\Sigma_J P(v,J)$ is the same as for our surprisal data. In addition, Fig. 14(a) also displays the experimental results of Gerrity and Valentini[11] for HD($v = 1$).

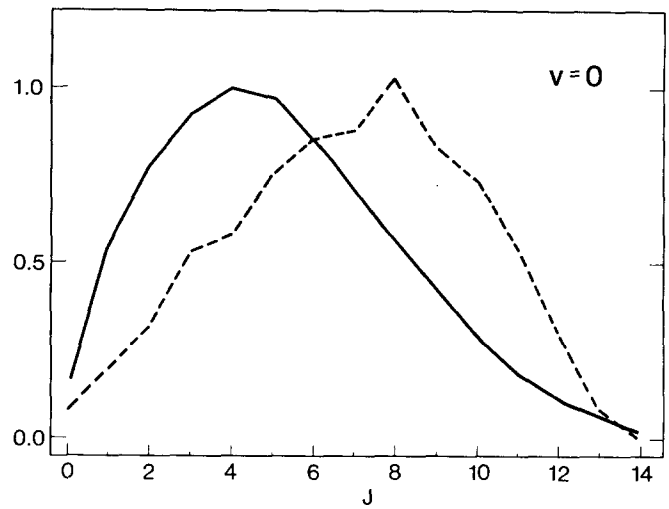

FIG. 15. HD($v = 0$) rotational distribution for the reaction of H + D_2. The solid curve represents an idealized distribution corresponding to a linear surprisal plot with a slope of $\theta_R = 4.9$ (see the text). The dashed curve indicates the results of Blais and Truhlar (Ref. 13).

These idealized distributions can be used to obtain an estimate of the relative vibrational state populations of HD($v = 1$) and HD($v = 2$). Using the measured ratios of HD($v = 1$, $J = 2$ and 3) to HD($v = 2$, $J = 2$ and 3) [see Eq. (1)] to provide for normalization, we obtain

$$\frac{\sum_J P(v=1,J)}{\sum_J P(v=2,J)} = 5.0 \pm 2.0 . \tag{8}$$

For completeness, Fig. 15 displays an idealized rotational distribution for HD($v = 0$) obtained by using $\theta_R = 4.9$, i.e., the average of that found for $v = 1$ and $v = 2$. Obviously, such an extrapolation cannot be made on rigorous grounds, but it is hoped that this distribution may serve as a guide to that expected for the HD($v = 0$) product formed only by collisions at ~ 1.30 eV. In comparing this distribution with those obtained by Blais and Truhlar[13] and Gerrity and Valentini,[11] it must be borne in mind that their distributions have a contribution from the ~ 0.55 eV collisions.

Why this fundamental reaction should lead to linear rotational surprisals is by no means obvious. Indeed, as remarked by Wyatt, "...a linear rotational surprisal is certainly not demanded in general by quantum mechanics. The results are the final step in a long road from Coulomb's law, via the Schrödinger equation..." [46] Schatz and Kupperman[48] have suggested that these temperature-like distributions may be a consequence of the restricted bending motion of the transition state, where a Gaussian wave packet, arising from the zero-point motion in the bend, becomes projected onto the free-rotor states of the diatomic product. However, while presenting a nice qualitative picture of the dynamics, this model does not quantitatively survive the transition from two to three dimensions.[5] Pollak[51] has suggested that linear rotational surprisals for the H + H_2 system arise as a consequence of a transform of momentum constraint, while Levine[52] has stated that linear rotational surprisals are expected when the amount of impulsive rotational energy release is

small. Along the same lines, Schatz and Ross[50] have shown that linear rotational surprisals can result from a generalized Franck–Condon model of the reaction dynamics. In this latter work it is demonstrated that linear surprisals arise when the potential surface dominates any kinematic coupling. However, linearity is *not* predicted at high rotational excitation. Indeed, since our data are restricted to $J \leqslant 6$, we do not know if the linearity will extend to the maximum J's populated.

Of course, linear surprisals are by no means confined to the $H + H_2$ family of reactions and are more the rule than the exception in dynamical studies.[52] That is not to say that this behavior can be rationalized. We believe that measurements for the $H + D_2$ system may be able to shed light on this phenomenon. A comprehensive study would require extention to other collision energies and include $HD(v = 0)$ and $J > 6$. In the absence of suitable experimental results, it would also be interesting to apply a surprisal analysis to quasiclassical trajectory results, for example. In particular, one may seek to learn at which point the kinematic coupling begins to dominate the H–D–D potential in controlling the product state distribution and what factors determine the slope.

C. Concluding remarks

A laser-based experimental procedure has been demonstrated for studying the detailed dynamics of the $H + D_2 \rightarrow HD + D$ reaction. Here the collision energy has been controlled using photolysis of HI, and both reaction products have been characterized using multiphoton ionization. The results obtained should provide a stringent test of detailed theories, even though the data have been limited to a single isotopic combination of reagents and to a single collision energy. The present study, together with the complementary work of Gerrity and Valentini,[11] should be regarded as only a first step on this road. We anticipate that the journey may be long but it will lead ultimately to a full understanding of the state-to-state dynamics of the $H + H_2$ family, the simplest of all bimolecular reactions.

Note added in proof: R. Götting, H. R. Mayne, and J. P. Toennies, J. Chem. Phys. (in press) have recently obtained angular and velocity distributions of HD formed in the crossed molecular beam reaction $D + H_2$ for an effective CM collision energy of ~ 1.0 eV. They also find a strong preference for product translational energy and report that the angular distribution changes from predominantly backward scattering at low energies to one that is essentially constant with angle for CM collision energies of ~ 2.0 eV. We thank J. P. Toennies for communicating these results to us prior to publication.

ACKNOWLEDGMENTS

We thank the Shell Companies Foundation, Inc., the U.S. Office of Naval Research under N00014-C-78-0403, the U.S. Air Force Office of Scientific Research under AFOSR F49620-83-C-0033, and the U.S. National Science Foundation under NSF CHE 80-06524 and NSF CHE 81-08823. We are also grateful for the loan of equipment from the San Francisco Laser Center, operated under NSF CHE 79-16250. We are also indebted to W. M. Huo for providing the relative two-photon transition probabilities for HD, and to R. S. Blake for experimental assistance.

APPENDIX: CENTER-OF-MASS COLLISION ENERGY

On photodissociation of stationary $HI(v = 0, J = 0)$ we have

$$h\nu = D_0^0(\mathrm{HI}) + E_{\mathrm{trans}} + E_e(I)\,, \tag{A1}$$

where $h\nu$ is the photon energy, $D_0^0(\mathrm{HI})$ the dissociation energy of $HI(v = 0, J = 0)$, E_{trans} is the kinetic energy of the H and I fragments, and E_e is the electronic energy of the I atom. At 266 nm, $h\nu = 4.661$ eV, while $D_0^0(\mathrm{HI})$ is 3.054 eV.[53] Conservation of momentum requires that the H atom carries off 99.22% of E_{trans}, while $E_e[\mathrm{I}(^2P_{3/2})] = 0$ and $E[\mathrm{I}(^2P_{1/2})] = 0.943$ eV.[55] Thus for the $\mathrm{I}(^2P_{3/2})$ channel, $V_{\mathrm{H}} = 17\,542$ m s^{-1}, and for $\mathrm{I}(^2P_{1/2})$, $V_{\mathrm{H}} = 11\,276$ m s^{-1}. When the rotational energy of the thermal HI is included, these velocities increase and acquire a considerable spread. We estimate $V_{\mathrm{H}} = 17\,660 \pm 120$ and $11\,460 \pm 180$ m s^{-1} for the two channels. Here an H atom velocity of magnitude $V_{\mathrm{H}}^{\perp}$ has been added at right angles to the recoil component, where

$$V_{\mathrm{H}}^{\perp} = \left[\frac{2\bar{E}_R}{M_{\mathrm{H}}(M_{\mathrm{HI}}/M_{\mathrm{I}})}\right]^{1/2} \tag{A2}$$

and $\bar{E}_R \simeq 22$ meV is the average HI rotational energy. Finally, we must include the thermal motion of the HI parent. This has a velocity of ~ 200 m s^{-1} at 300 K, directed randomly with respect to the H atom recoil direction. This adds a spread $\sim \pm 170$ m s^{-1} to v_{H}. Thus we obtain $v_{\mathrm{H}} = 17\,660 \pm 290$ and $11\,460 \pm 350$ m s^{-1} for the two dissociation channels, where the bounds extend approximately to the half maximum points. Actually, in these calculations, we require $\bar{V}_{\mathrm{H}}^2$ which is increased by the thermal velocity of the HI. However, the magnitude of this effect is negligible (< 2 m s^{-1}) for a most probable HI thermal velocity ~ 200 m s^{-1}.

The mean center-of-mass collision energy $\bar{E}_{\mathrm{CM}}$ is given by

$$\bar{E}_{\mathrm{CM}} = \tfrac{1}{2}\mu\,\bar{V}_{\mathrm{rel}}^2\,, \tag{A3}$$

where μ is the reduced mass of the H, D_2 system and is equal to 4/5 amu, while $\bar{V}_{\mathrm{rel}}^2$ is the average square of the relative velocity of the reagents. At a collision angle of θ,

$$V_{\mathrm{rel}}^2 = V_{\mathrm{H}}^2 + V_{\mathrm{D_2}}^2 - 2V_{\mathrm{H}}V_{\mathrm{D_2}}\cos\theta\,, \tag{A4}$$

where $V_{\mathrm{D_2}}$ is the D_2 velocity. For a Maxwell–Boltzmann distribution of $V_{\mathrm{D_2}}$ given by

$$f(V)dV \propto V^2 \exp[-V^2 M(\mathrm{D_2})/2kT]\,dV \tag{A5}$$

we find, after averaging V_{rel}^2 over all angles and D_2 velocities that

$$\bar{V}_{\mathrm{rel}}^2 = V_{\mathrm{H}}^2 + \frac{3}{2}\left(\frac{2kT}{M(\mathrm{D_2})}\right), \tag{A6}$$

where we have ignored the spread in V_{H}. From Eqs. (A3) and (A6) we obtain for the $H + \mathrm{I}(^2P_{3/2})$ channel

$$\bar{E}_{\mathrm{CM}}(H + D_2) = 1.30 \pm 0.04 \text{ eV} \tag{A7a}$$

and for the $H + I(^2P_{1/2})$ channel

$$\overline{E}_{CM}(H + D_2) = 0.55 \pm 0.03 \text{ eV} . \quad \text{(A7b)}$$

[1]F. London, Z. Elektrochem. **35**, 552 (1929).
[2]H. Eyring and M. Polanyi, Z. Phys. Chem. Abt. B **12**, 279 (1931). See also H. Pelzer and E. P. Wigner, *ibid.* **15**, 445 (1932).
[3]For reviews see D. G. Truhlar and R. E. Wyatt, Annu. Rev. Phys. Chem. **27**, 1 (1976); M. Baer, Adv. Chem. Phys. **49**, 191 (1982).
[4]P. Siegbahn and B. Liu, J. Chem. Phys. **68**, 2457 (1978); D. G. Truhlar and C. J. Horowitz, *ibid.* **68**, 2466 (1978); **71**, 1514 (1979).
[5]G. C. Schatz and A. Kuppermann, J. Chem. Phys. **62**, 2502 (1975); **65**, 4642, 4668 (1976).
[6]A. B. Elkowitz and R. E. Wyatt, J. Chem. Phys. **62**, 2504 (1975); **63**, 702 (1975).
[7]R. B. Walker, E. B. Stechel, and J. C. Light, J. Chem. Phys. **69**, 2922 (1978).
[8]*State-to-State Chemistry*, edited by P. R. Brooks and E. F. Hayes, ACS Symp. Ser. No. 56 (American Chemical Society, Washington, D.C. 1977).
[9]J. C. Whitehead, Comp. Chem. Kinet. **24**, 357 (1982).
[10]M. R. Levy, Prog. React. Kinet. **10**, 1 (1979).
[11]D. P. Gerrity and J. J. Valentini, J. Chem. Phys. **79**, 5202 (1983).
[12]C. T. Rettner, E. E. Marinero, and R. N. Zare, in *Physics of Electronic and Atomic Collisions*, edited by J. Eichler, I. V. Hertel, and N. Stolterfoht (North-Holland, Amsterdam, 1984), p. 51.
[13]N. C. Blais and D. G. Truhlar, Chem. Phys. Lett. **102**, 120 (1983).
[14]R. G. W. Norrish and G. Porter, Nature **164**, 685 (1950); G. Porter, Proc. R. Soc. London Ser. A **200**, 284 (1950); R. J. Donovan and H. M. Gillespie, in *A Specialist Periodical Report: Reaction Kinetics*, edited by P. R. Ashmore (Chemical Society, London, 1975), Vol. 1, Chap. 1, pp. 14–92.
[15]A. C. Luntz, R. Schinke, W. A. Lester, Jr., and Hs. H. Günthard, J. Chem. Phys. **70**, 5908 (1979).
[16]G. K. Smith and J. E. Butler, J. Chem. Phys. **73**, 2243 (1980).
[17]W. H. Breckenridge and H. Umemoto, J. Chem. Phys. **75**, 4153 (1981).
[18]J. F. Córdova, C. T. Rettner, and J. L. Kinsey, J. Chem. Phys. **75**, 2742 (1981).
[19]R. R. Williams, Jr. and R. A. Ogg, Jr., J. Chem. Phys. **15**, 691 (1947).
[20]H. A. Schwarz, R. R. Williams, Jr., and W. H. Hamill, J. Am. Chem. Soc. **74**, 6007 (1952); R. J. Carter, W. H. Hamill, and R. R. Williams, Jr., *ibid.* **77**, 6457 (1955).
[21]R. M. Martin and J. E. Willard, J. Chem. Phys. **40**, 3007 (1964).
[22]A. Kupperman and J. M. White, J. Chem. Phys. **44**, 4352 (1966); A. Kuppermann, Isr. J. Chem. **7**, 303 (1969). See also L. A. Melton and R. G. Gordon, J. Chem. Phys. **51**, 5449 (1969).
[23]C. R. Quick, Jr., R. E. Weston, Jr., and G. W. Flynn, Chem. Phys. Lett. **83**, 15 (1981).
[24]F. Magnotta, D. J. Nesbitt, and S. R. Leone, Chem. Phys. Lett. **83**, 21 (1981); C. A. Wight and S. R. Leone, J. Chem. Phys. **78**, 4875 (1983).
[25]C. F. Wood, G. W. Flynn, and R. E. Weston, Jr., J. Chem. Phys. **77**, 4776 (1982).
[26]C. R. Quick, Jr., and D. S. Moore, J. Chem. Phys. **79**, 759 (1983).
[27]E. E. Marinero, C. T. Rettner, and R. N. Zare, Phys. Rev. Lett. **48**, 1323 (1982).
[28]E. E. Marinero, R. Vasudev, and R. N. Zare, J. Chem. Phys. **78**, 692 (1983).
[29]J. W. Nibler, J. R. McDonald, and A. B. Harvey, Opt. Commun. **18**, 371 (1976).
[30]M. Péalat, J.-P. E. Taran, J. Taillet, M. Bacal, and A. M. Bruneteau, J. Appl. Phys. **52**, 2687 (1981).
[31]M. Péalat, D. Debarre, J.-M. Marie, J.-P. E. Taran, A. Tramer, and C. B. Moore, Chem. Phys. Lett. **98**, 299 (1983).
[32]E. E. Marinero, C. T. Rettner, R. N. Zare, and A. H. Kung, Chem. Phys. Lett. **95**, 486 (1983); C. T. Rettner, E. E. Marinero, R. N. Zare, and A. H. Kung, J. Phys. Chem. (in press).
[33]F. J. Northrup, J. C. Polanyi, S. C. Wallace, and J. M. Williamson, Chem. Phys. Lett. **105**, 34 (1984).
[34]L. Åsbrink, Chem. Phys. Lett. **7**, 549 (1970).
[35]A. Niehaus and M. W. Ruf, Chem. Phys. Lett. **11**, 55 (1971).
[36]J. E. Pollard, D. J. Trevor, J. E. Reutt, Y. T. Lee, and D. A. Shirley, Chem. Phys. Lett. **88**, 434 (1982); J. Chem. Phys. **77**, 34 (1982); J. E. Pollard, D. J. Trevor, Y. T. Lee, and D. A. Shirley, *ibid.* **77**, 4818 (1982).
[37]D. J. Kligler and C. K. Rhodes, Phys. Rev. Lett. **40**, 309 (1978); D. J. Kligler, J. Bokor, and C. K. Rhodes, Phys. Rev. A **21**, 607 (1980).
[38]J. Romand, Ann. Phys. **4**, 527 (1949).
[39]R. Schmiedl, H. Dugan, W. Meier, and K. H. Welge, Z. Phys. A **304**, 137 (1982).
[40]G. N. A. van Veen, K. A. Mohamed, T. Baller, and A. E. de Vries, Chem. Phys. **80**, 113 (1983).
[41]R. D. Clear, S. J. Riley, and K. R. Wilson, J. Chem. Phys. **63**, 1340 (1974).
[42]G. C. Bjorklund, C. P. Ausschnitt, R. R. Freeman, and R. H. Storz, Appl. Phys. Lett. **33**, 54 (1978).
[43]A. Sepehrad, R. M. Marshall, and H. Purnell, Int. J. Chem. Kinet. **11**, 411 (1979).
[44]W. M. Huo (private communication).
[45]G.-D. Barg, H. R. Mayne, and J. P. Toennies, J. Chem. Phys. **74**, 1017 (1981).
[46]R. E. Wyatt, Chem. Phys. Lett. **34**, 167 (1975).
[47]M. J. Redmon and R. E. Wyatt, Int. J. Quantum Chem. Symp. **9**, 403 (1975).
[48]G. C. Schatz and A. Kuppermann, J. Chem. Phys. **65**, 4624 (1976).
[49]R. B. Bernstein, Int. J. Quantum Chem. Symp. **10**, 267 (1976).
[50]G. C. Schatz and J. Ross, J. Chem. Phys. **66**, 2943 (1977).
[51]E. Pollak, Chem. Phys. Lett. **47**, 513 (1977).
[52]R. D. Levine, B. R. Johnson, and R. B. Bernstein, Chem. Phys. Lett. **19**, 1 (1973). For reviews of the information-theoretic approach to data analysis see: R. D. Levine, Annu. Rev. Phys. Chem. **29**, 59 (1978); R. B. Bernstein and R. D. Levine, Adv. At. Mol. Phys. **11**, 215 (1975); R. D. Levine and J. L. Kinsey, in *Atom-Molecule Collision Theory, A Guide for the Experimentalist*, edited by R. B. Bernstein (Plenum, New York, 1979), p. 693.
[53]K. P. Huber and G. Herzberg, *Molecular Spectra and Molecular Structure IV. Constants of Diatomic Molecules* (Van Nostrand Reinhold, New York, 1979).
[54]I. Dabrowski and G. Herzberg, Can. J. Phys. **54**, 525 (1976).
[55]C. E. Moore, Natl. Bur. Stand. (U.S.) Circ. 467 (1958) Vol. 3.